1993ApJ...417...82E

THE ASTROPHYSICAL JOURNAL, 417:82–89, 1993 November 1
© 1993. The American Astronomical Society. All rights reserved. Printed in U.S.A.

HUBBLE SPACE TELESCOPE IMAGING OF THE NARROW-LINE REGION OF NGC 4151

I. N. EVANS,[1] Z. TSVETANOV,[2] G. A. KRISS,[2] H. C. FORD,[1,2] S. CAGANOFF,[2,3] AND A. P. KORATKAR[1]

Received 1993 January 20; accepted 1993 May 7

ABSTRACT

We have used the Planetary Camera aboard the *Hubble Space Telescope* to obtain high spatial resolution [O III] λ5007 and Hα λ6563+[N II] λλ6548, 6583 images of the nucleus of NGC 4151. Almost all of the Hα λ6563+[N II] λλ6548, 6583 emission arises from an unresolved nuclear point source. The [O III] λ5007 image resolves the narrow-line region into a number of emission-line clouds distributed in a biconical structure with apices coincident with a central point source, a projected opening angle of 75° ± 10°, and a projected axis oriented along P.A. 60°/240° ± 5°. The position angle of the [O III] λ5007 emission is aligned with the extension of the nuclear VLBI radio source. We infer from these data a geometry of the narrow-line region that places our line of sight outside the ionization cones. The simultaneous presence of a nearly unobscured UV/optical continuum, a central pointlike broad-line region, and a biconical ionization geometry argues that the simplest version of the unified model that invokes a very optically thick molecular torus surrounding the BLR to collimate the nuclear ionizing radiation does not apply to this object. We consider several alternative collimation mechanisms that are compatible with our data as well as with column densities inferred from the UV absorption lines and from the X-ray spectrum.

Subject headings: galaxies: individual (NGC 4151) — galaxies: nuclei — galaxies: Seyfert

1. INTRODUCTION

In recent years, observational differences between various types of active galactic nuclei have been successfully interpreted in terms of anisotropy and orientation effects. The basic hypothesis that is the cornerstone of the now commonly accepted unified model for these objects is that the optical, UV, and probably soft X-ray radiation is emitted anisotropically from the nucleus into two wide, oppositely directed ionization cones, presumably through shadowing by an optically thick disk or torus that collimates the ionizing radiation field (e.g., Lawrence & Elvis 1982; Lawrence 1987; Barthel 1989). The major consequence of this hypothesis is that many observational characteristics, such as the widths of the recombination lines, and optical and UV luminosities, are aspect dependent. In particular, Seyfert 1 nuclei and other broad emission-line objects (such as quasars) correspond to a line of sight that falls within the solid angle subtended by one of the ionization cones, so that the observer sees directly the inner regions where the broad lines and ionizing continuum are produced. In contrast, the line of sight to Seyfert 2 and other objects lacking broad emission lines (for example, narrow line radio galaxies) lies outside of the ionization cones, so that the ionizing continuum source and the broad-line region (BLR) are obscured from direct visibility.

Observational support for the unified model of active galactic nuclei has come mainly from two directions. Spectropolarimetric studies have revealed broad lines and other Seyfert 1 features in the radiation from Seyfert 2 nuclei that has been scattered off the local interstellar medium. Antonucci & Miller (1985) proposed a model for the prototypical Seyfert 2 galaxy NGC 1068 in which a very optically thick molecular torus surrounds the nuclear engine. In their model, radiation from the hidden Seyfert 1 nucleus is scattered by a hot electron cloud above the torus and is visible only in polarized light. This model has been developed theoretically by Krolik & Begelman (1986) and Krolik & Lepp (1989). Miller & Goodrich (1990) found that at least four of eight Seyfert 2 galaxies observed spectropolarimetrically show evidence for the presence of a hidden Seyfert 1 nucleus. Morphological studies also support the hypothesis that the primary difference between the nuclei of Seyfert 1 and 2 galaxies results from orientation effects. Narrow-band imaging observations demonstrate that Seyfert 1 nuclei have predominantly compact morphologies, whereas Seyfert 2 galaxies tend to have ionized gas structures that show elongated and in some cases biconical morphologies for the extended emission-line region (e.g., Wilson, Ward, & Haniff 1988; Pogge 1989; Tadhunter & Tsvetanov 1989), as well as the near-UV continuum (Pogge & de Robertis 1992; Kriss et al. 1993).

The bright northern emission-line galaxy NGC 4151 has been classified as a type 1.5 Seyfert galaxy by Osterbrock & Koski (1976) because of the presence of both broad permitted lines and prominent narrow forbidden lines in the optical spectrum. Several recent imaging and spectroscopic studies (e.g., Ulrich 1973; Heckman & Balick 1983; Schulz 1987, 1988, 1990; Pérez et al. 1989; Penston et al. 1990; Pérez-Fournon & Wilson 1990; Terlevich et al. 1991) have demonstrated that the broad-line emission is produced by a point-source nuclear component which is surrounded by an extended region of narrow forbidden-line emission which is elongated in the NE–SW direction.

In this paper, we present narrow-band [O III] λ5007 and Hα λ6563+[N II] λλ6548, 6583 imaging of the innermost portion of the narrow-line region (NLR) obtained using the *Hubble Space Telescope* (*HST*), and examine the implications of these data for models of the anisotropy of the ionizing radiation in NGC 4151.

[1] Space Telescope Science Institute, 3700 San Martin Drive, Baltimore, MD 21218.
[2] Center for Astrophysical Sciences, Department of Physics and Astronomy, Johns Hopkins University, Baltimore, MD 21218.
[3] School of Physics, University of Melbourne, Parkville, Victoria 3052, Australia.

© American Astronomical Society • Provided by the NASA Astrophysics Data System

1993ApJ...417...82E

2. OBSERVATIONS AND REDUCTIONS

The images reported in this paper were obtained on 1991 June 18/19 using the Planetary Camera (PC) configuration of the Wide Field and Planetary Camera (WFPC) on-board *HST*. A narrow-band image in each of the [O III] λ5007 and Hα λ6563 + [N II] λλ6548, 6583 emission lines was obtained using the F502N (nominal mean wavelength/effective width 5018/29 Å) and F664N (6637/131 Å) filters, and a continuum image was obtained using the F547M (5454/438 Å) filter. The total exposure times in these filters were 1608, 400, and 350 s, respectively. The spacecraft fine lock tracking mode was used throughout the observations, with a single loss-of-lock event occurring during the F502N integration which reduced the exposure time from the nominal value of 1800 s. The rms pointing jitter values for the F502N, F664N, and F547M exposures are 5.5, 3.7, and 3.6 milliarcseconds, respectively.

After the data were obtained, they were automatically processed by the WFPC Routine Science Data Processing pipeline at the Space Telescope Science Institute. The pipeline calibrations applied to the data follow the precepts of Lauer (1989), and include masking known bad pixels, A/D correction to allow for the faulty WFPC A/D converter, bias level removal and bias image subtraction, preflash image scaling and subtraction, dark image scaling and subtraction, and flat-field correction. The calibrated [O III] λ5007 (F502N), Hα λ6563 + [N II] λλ6548, 6583 (F664N), and continuum (F547M) images of the nuclear region, rotated so that north is up, are presented in Figures 1–3 (Plates 1–4). The central point source visible in the figures was saturated during the exposures, resulting in charge bleeding along the column direction of the CCD. In Figure 4 (Plate 5) we provide a ground-based continuum-subtracted Hα λ6563 image of the galaxy for comparison purposes to aid the reader. The ground based images were obtained using the RCA No. 3 CCD camera at the f/7.5 focus of the No. 1, 36 inch telescope at Kitt Peak National Observatory on the night of 1985 April 16/17 under near photometric conditions. Exposures of 300 s through the 6606/75 (nominal mean wavelength/effective width 6606/75 Å) filter, and 450 s through the 6200/450 filter, provide the Hα λ6563 and continuum images, respectively.

Following pipeline processing, the *HST* images were registered by translating the narrow-band frames until the core of the point spread function (PSF) arising from the nuclear point source was aligned to better than ∼0.1 pixel in x and y between the three images. The core of the PSF from the nuclear point source was the only feature common to all frames that could be used for registration purposes. The distributions of the [O III] λ5007 and Hα λ6563 + [N II] λλ6548, 6583 emission-line excesses are shown in Figures 5 and 6, where we symbolically present the normalized ratio of the flux observed through the narrow-band filter (F502N and F664N) to the flux observed through the continuum filter (F547M). In these figures, the filter fluxes have been summed over 0.″3 × 0.″3 square apertures, and are normalized so that the ratio of the fluxes through the aperture centered on the nuclear point source (but excluding the contribution of the saturated pixels) is arbitrarily set to unity. Inspection of these figures shows immediately that the emission-line gas is distributed in an approximately NE–SW orientation on either side of the nuclear point source, and that the emission-line intensities are largest to the SW of the nucleus. If the nuclear emission-line regions are located symmetrically about the nucleus, this may imply that the extinction to the NE emission-line region is greater than the extinction to the the SW emission-line region.

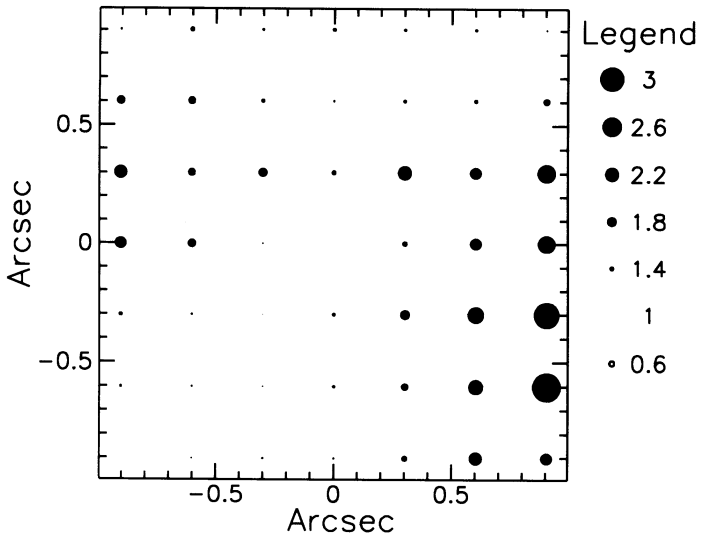

FIG. 5.—Ratios of the normalized F502N to F547M fluxes, integrated through a 0.″3 × 0.″3 aperture.

After aligning the data frames, the large scale continuum structure was removed from the narrow-band images by subtracting a suitably scaled version of the registered continuum frame. The scale factor was determined by requiring that the contribution of the stellar disk be eliminated in two regions, each approximately 1″ × 1″ in size, located symmetrically about the nucleus at a radius of ∼4″ along P.A. 150°/330° (i.e., perpendicular to the axis of the [O III] λ5007 emission).

To correct for the spatial blurring introduced by the spherical aberration present in the *HST* optics, we have deconvolved a region of the continuum-subtracted [O III] λ5007 image centered on the nucleus using both the Richardson-Lucy algorithm (Richardson 1972; Lucy 1974) and the MEMSYS5 quantified maximum entropy software package (Gull & Skilling 1991). The maximum entropy method (MEM) deconvolu-

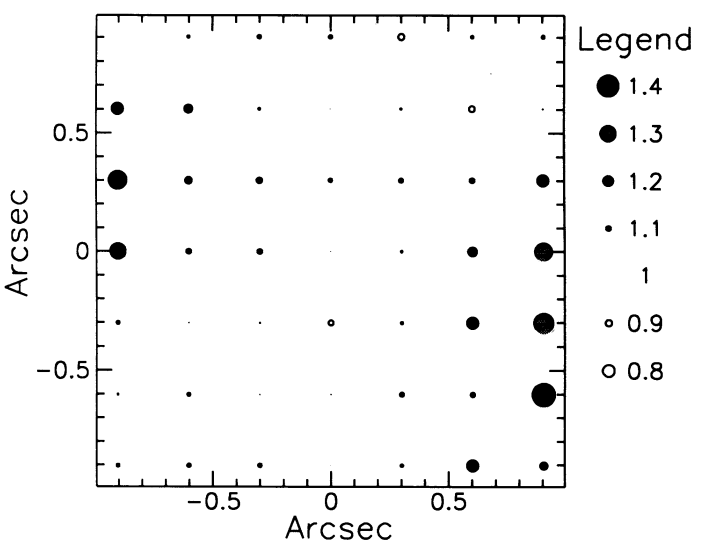

FIG. 6.—Same as Fig. 5, except that the F664N to F547M flux ratios are shown.

© American Astronomical Society • Provided by the NASA Astrophysics Data System

1993ApJ...417...82E

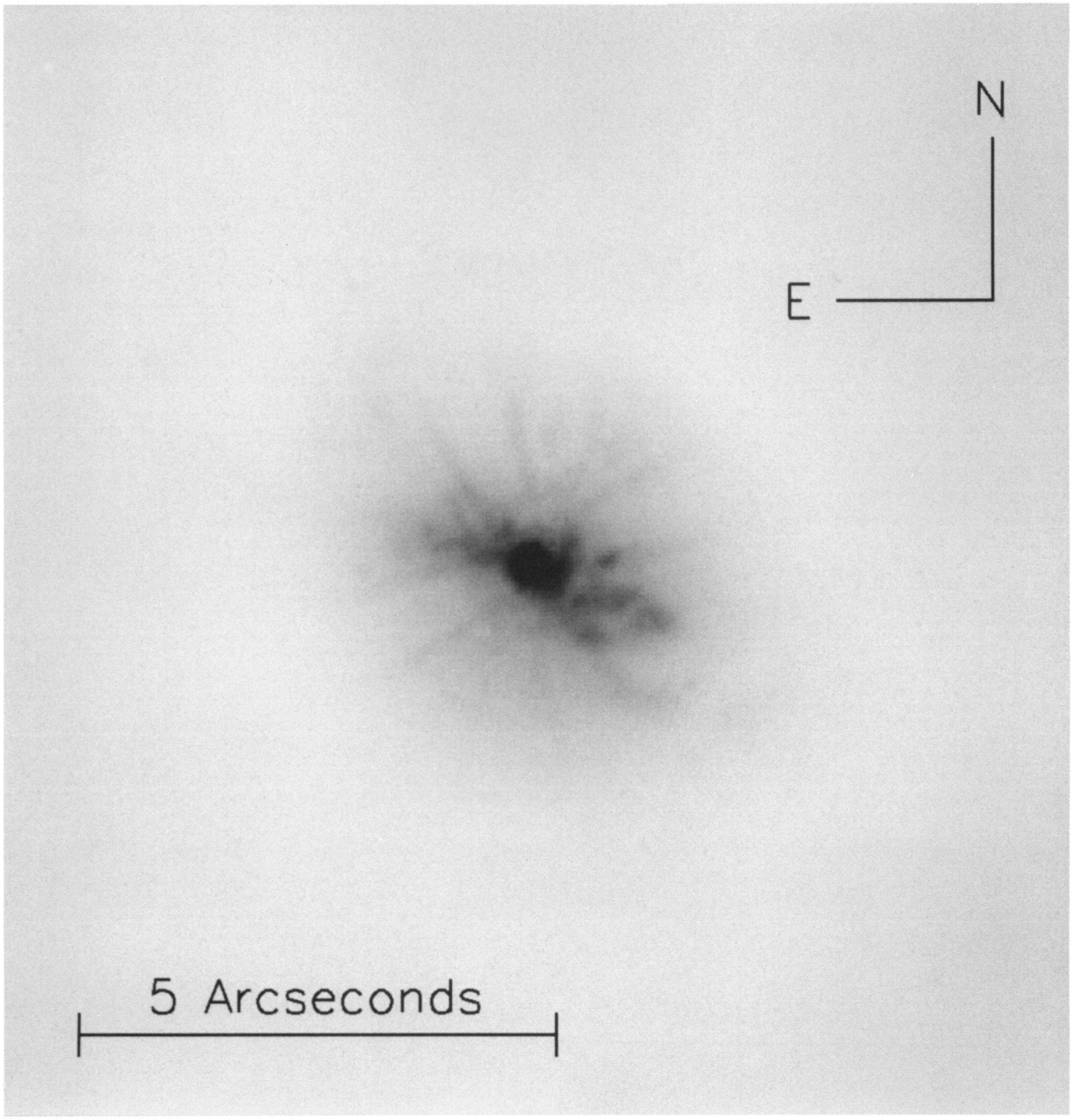

FIG. 1a

FIG. 1.—(*a*) [O III] λ5007 image of the nuclear region of NGC 4151 obtained through the PC F502N filter, scaled by a square root function between 0% and 100% of the peak intensity of the extended emission (i.e. excluding the central saturated point source). (*b*) same as (*a*), except that the image is linearly scaled between 0% and 25% of the peak intensity of the extended emission.

© American Astronomical Society • Provided by the NASA Astrophysics Data System

1993ApJ...417...82E

PLATE 2

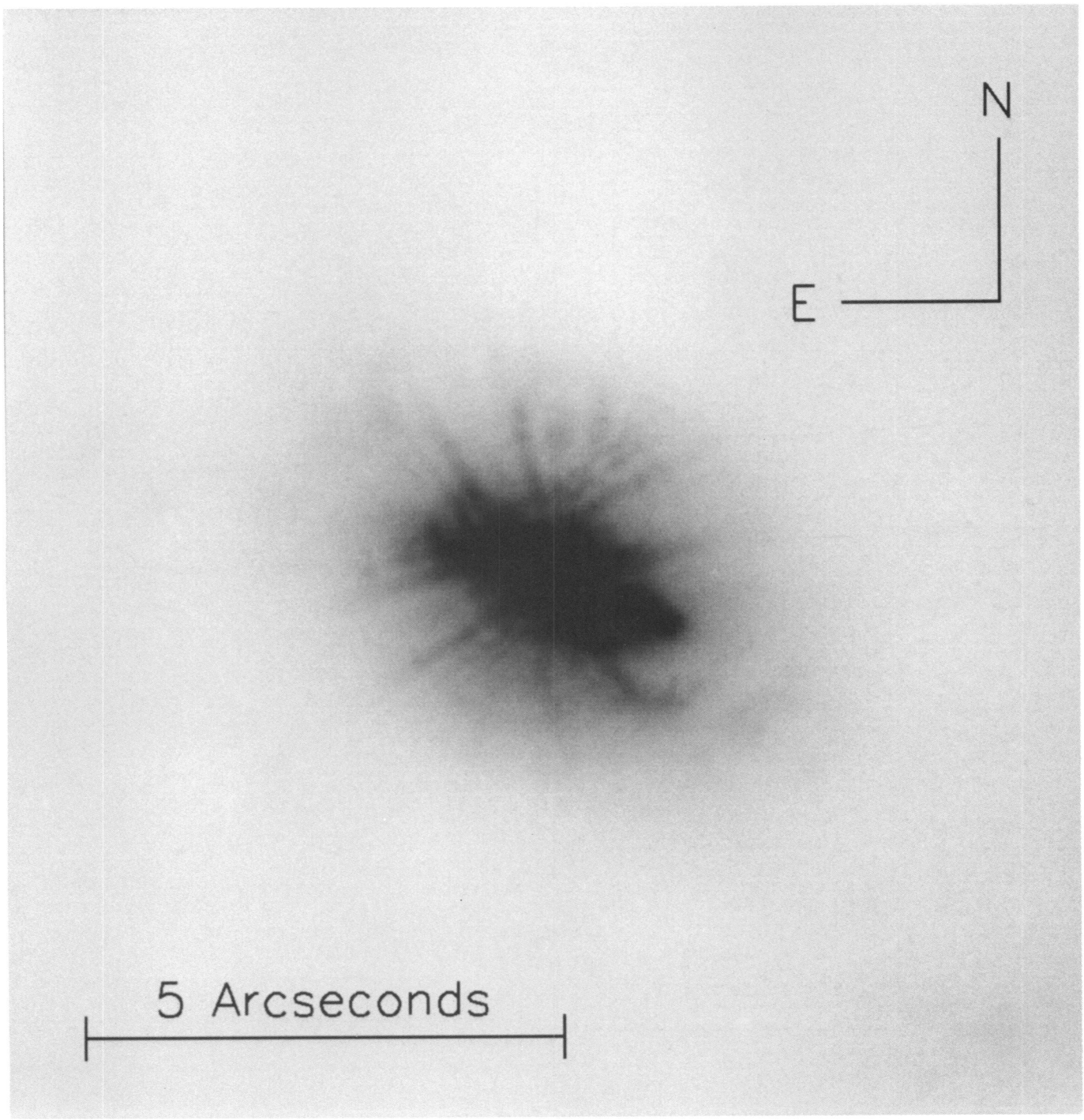

FIG. 1*b*

EVANS et al. (see 417, 83)

© American Astronomical Society • Provided by the NASA Astrophysics Data System

1993ApJ...417...82E

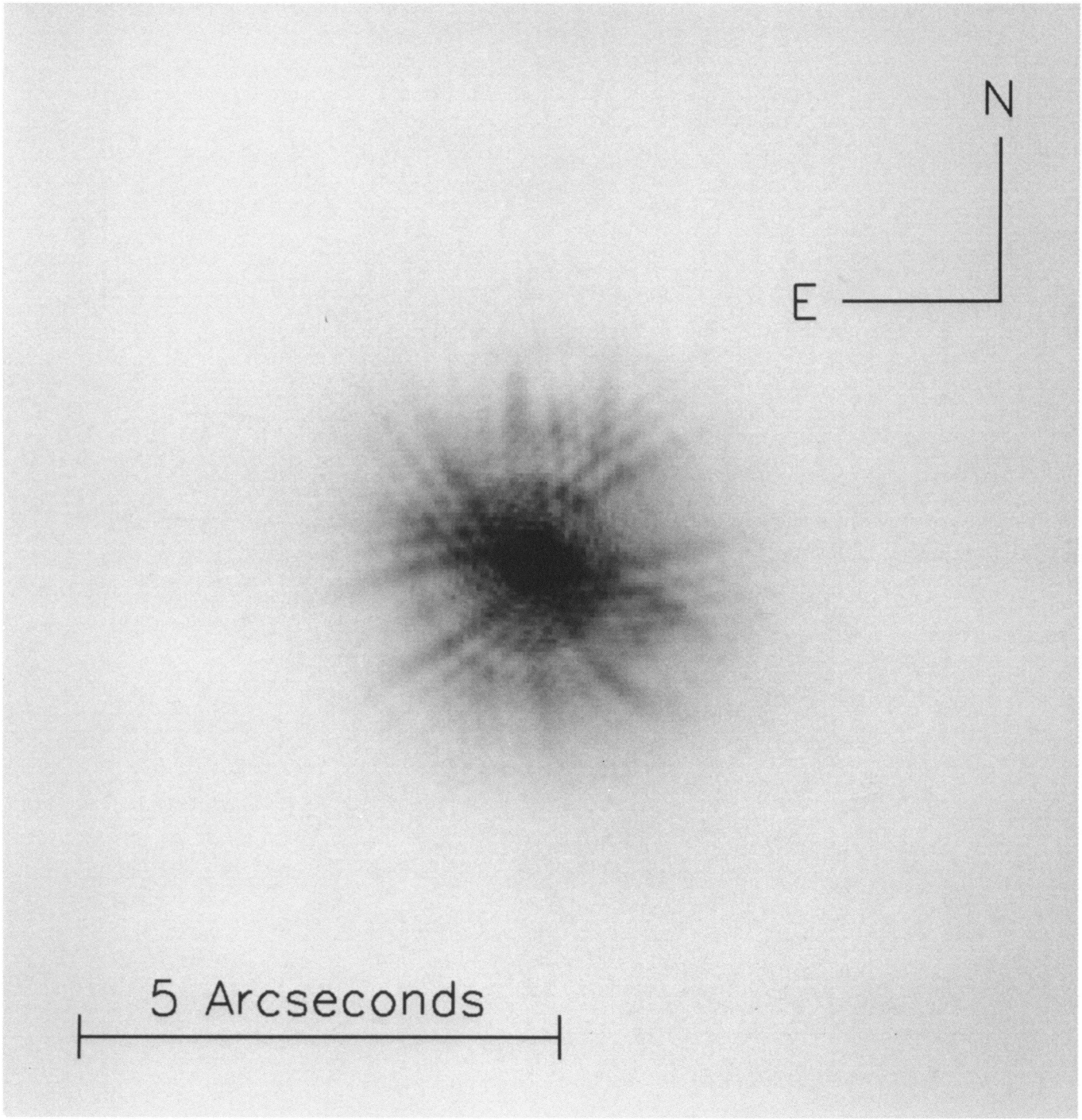

FIG. 2.—Same as Fig. 1*a*, except that the Hα λ6563 + [N II] λλ6548, 6583 image obtained through the F664N filter is shown

© American Astronomical Society • Provided by the NASA Astrophysics Data System

1993ApJ...417...82E

PLATE 4

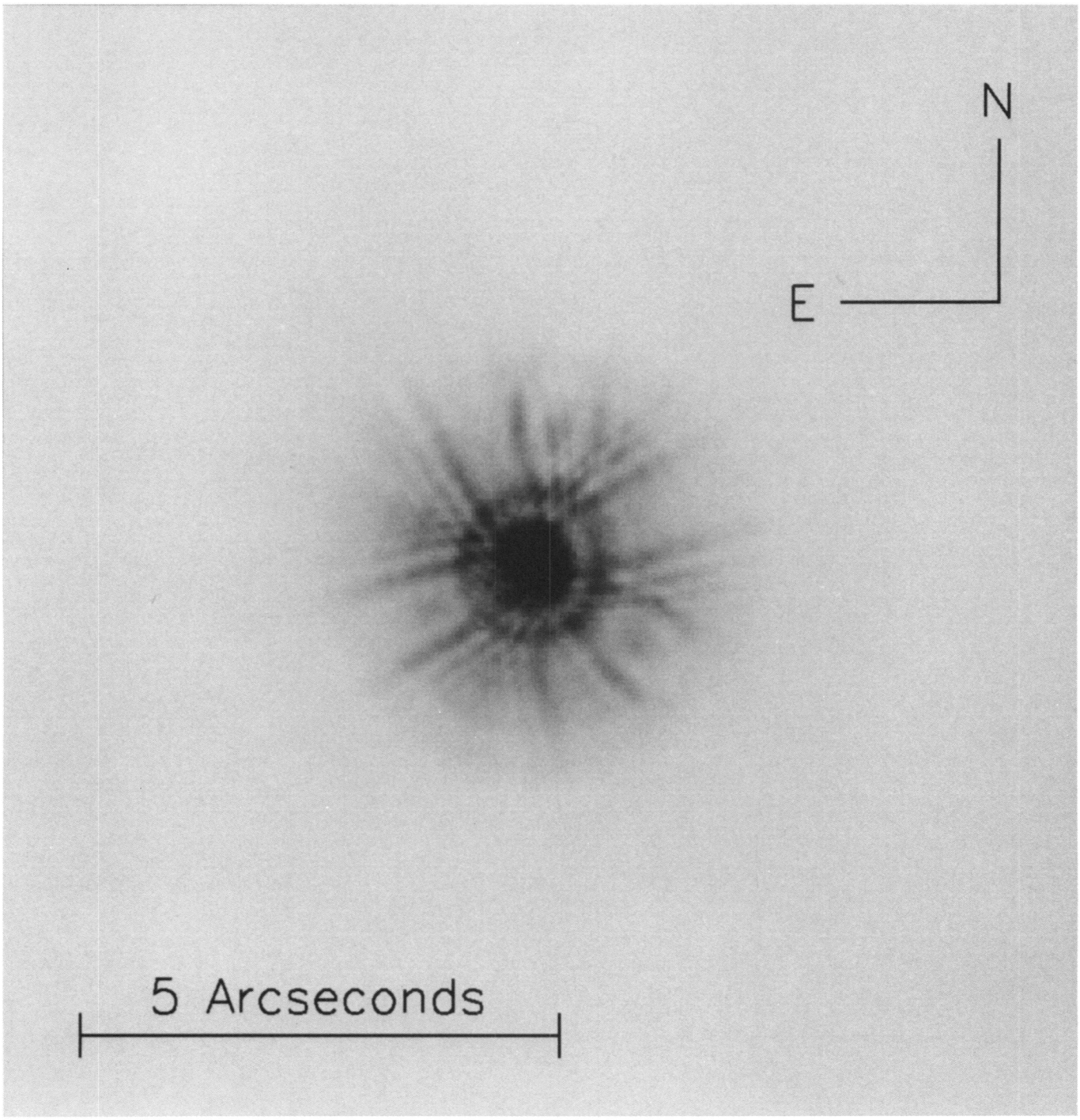

FIG. 3.—Same as Fig. 1*a*, except that the continuum image obtained through the F547M filter is shown

© American Astronomical Society • Provided by the NASA Astrophysics Data System

1993ApJ...417...82E

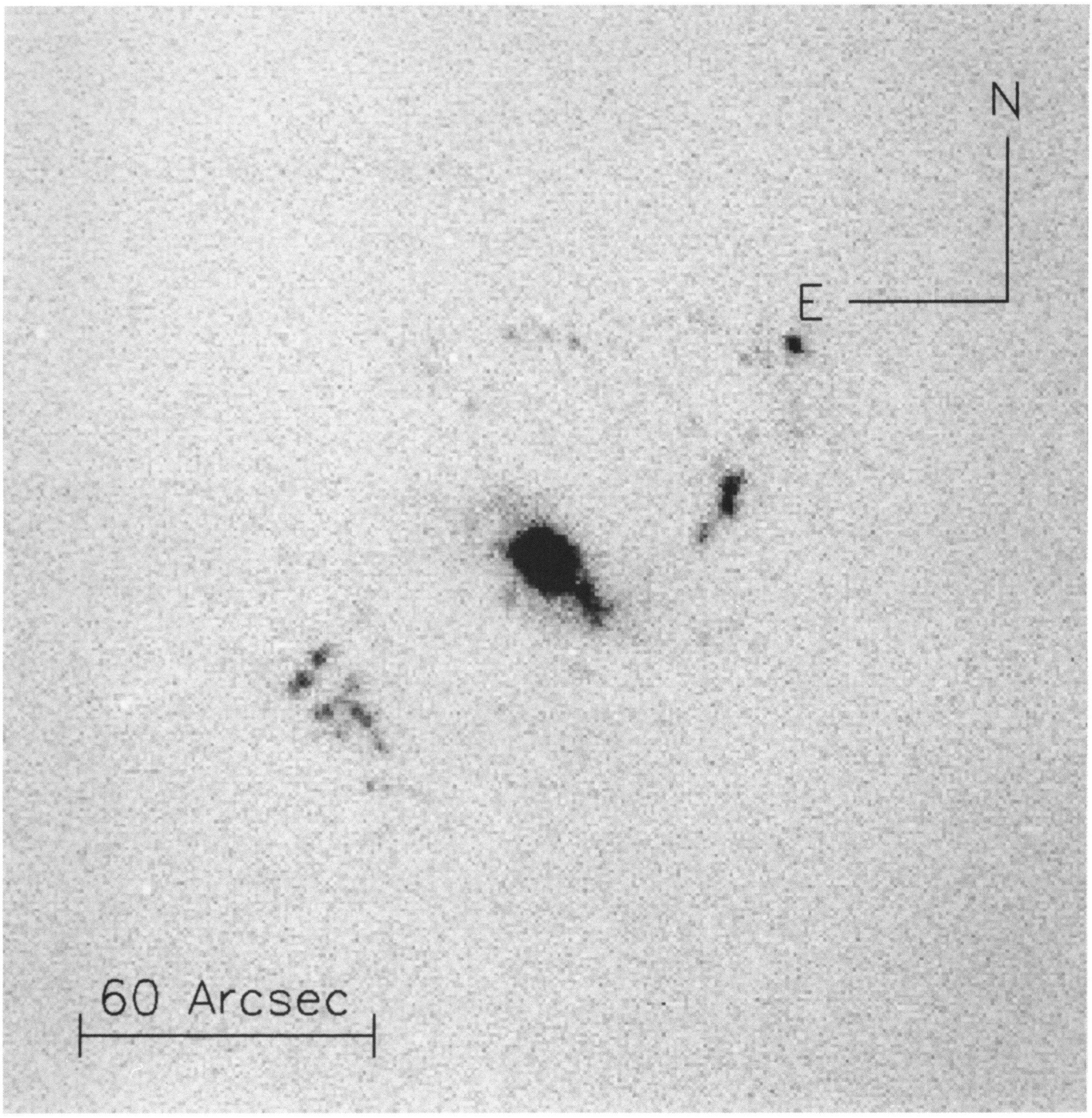

FIG. 4.—Ground-based continuum subtracted Hα λ6563 image of NGC 4151

© American Astronomical Society • Provided by the NASA Astrophysics Data System

1993ApJ...417...82E

tion was performed using an identical technique to that employed by Evans et al. (1991). Both a theoretical model PSF and an empirical PSF were used to deconvolve the data. The Tiny Tim software package (Krist 1992) was used to compute a model of the PSF that would be observed through the F502N filter at the same location on the PC CCD, and with the same pointing jitter, as the observations. The central region of the F547M image of the nucleus, which appears to be an unresolved point source atop a faint, smooth galaxy background, was used as the basis of the empirical PSF. However, because the core of the PSF from the F547M image was saturated, the final empirical PSF was constructed by grafting the core from the Tiny Tim model to the observed F547M wings after first normalizing the total intensity in the model wings to the total intensity in the observed wings.

The Richardson-Lucy reconstruction of the continuum-subtracted [O III] λ5007 image of the nuclear region is presented in Figure 7 (Plates 6–7), while the final MEM solutions are shown in Figures 8 (Plates 8–9) and 9 (Plates 10–11). Only the reconstructions computed using the theoretical model PSF are shown; the reconstructions computed using the empirical PSF are identical except in the very inner region surrounding the bright central peak. As discussed above, the central source visible in the figures was saturated during the F502N exposure, resulting in charge bleeding along the column direction of the CCD. Unfortunately, because of the surrounding emission from the NLR clouds, the precise distribution of flux in the central point source cannot be accurately determined. In the deconvolved images this uncertainty is manifested through an artificially complex reconstructed profile for the central point source. This is most easily visible in Figure 9*a* where the central point source seems to have a double structure, and Figure 9*b* where it has a scalloped appearance.

A further consequence of the CCD saturation and charge bleeding is that the total flux contained in the core of the saturated profile cannot be estimated accurately from the wings of the PSF. It is therefore not possible to completely remove the wings of the PSF associated with the central point source feature given the information contained in the raw image. The saturated central source introduces additional spurious details into the reconstruction near the nucleus that are most noticeable as a pair of faint "rings" of apparent emission centered on the bright nuclear source. These rings coincide with similar features visible in the PSF. However, without further observations we cannot tell unambiguously if the rings are *completely* spurious artifacts of the reconstruction or whether some fraction of the flux results from real features in the galaxy. Experience gained from image reconstruction of other bright point sources superposed on faint backgrounds with the *HST* PSF *suggests*, however, that the rings are artifacts of the reconstruction.

The remaining features evident in the reconstructed images do not correlate with the distribution of flux in the wings of the PSF associated with the central point source, and it is highly unlikely that they are artifacts of the reconstruction. Almost all of the individual features that can be identified in Figures 7–9 are clearly visible in all three of the separate reconstructed images, and many are identifiable in the original raw [O III] λ5007 image (Fig. 1). This correlation provides confidence in the reconstructions and can be used to assess the reality of specific features in the reconstructed images. We estimate from the FWHM of the narrowest features in the reconstruction that the resolution is $\sim$0.″085.

3. DISCUSSION

3.1. *Emission-Line Morphology*

Inspection of the figures reveals that the [O III] λ5007 gas found in the nucleus of NGC 4151 is distributed in a biconical structure with apices coincident with a bright central pointlike source. The emission-line regions themselves form a knotty, stringlike structure rather than a group of discrete narrow-line clouds, with the individual filaments being extended over lengths of up to $\sim$0.″4 ($\sim 20\ h$ pc; $H_0 = 100\ h^{-1}$ km s^{-1} Mpc^{-1}), implying that the filaments are themselves spatially resolved. The stringlike structure that is present in the emission-line gas is also visible at larger radii from the central nuclear source in ground-based images of the extended narrow-line region (ENLR; Pérez-Fournon & Wilson 1990), suggesting that the physical mechanisms which form the clouds in the NLR close to the nucleus are similar to those in the ENLR.

The most striking feature of the observed morphology of the [O III] λ5007 gas is its clearly biconical distribution. Both emission-line cones share the same axis position angle and have identical opening angles to within the measurement errors. With the exception of a slight northern protrusion immediately to the SW of the central source, both cones exhibit relatively hard edges outside of which there is very little emission. We measure a cone opening angle projected on the plane of the sky of $75° \pm 10°$, with a projected axis P.A. of $60°/240° \pm 5°$. The measured cone opening angle is wider than would be inferred from the distribution of emission-line gas at larger radii in the ENLR (Heckman & Balick 1983; Pérez et al. 1989; Penston et al. 1990; Pérez-Fournon & Wilson 1990; Schulz 1990; Terlevich et al. 1991). However, we note that when projected onto the plane of the sky, all the extended emission-line gas appears to be contained completely in the sector of the sky generated by extending the observed near-nuclear radiation cone to the radius of the ENLR. This natural extension of the [O III] λ5007 emission-line cones observed with *HST* to the emission-line gas found in the near-nuclear NLR and ENLR observed from the ground suggests very strongly that the extended emission-line gas is encapsulated *physically* within the volume of space generated by extending the nuclear cones to greater radii.

Our data reveal that there is essentially no line emission visible in either of the [O III] λ5007 or Hα λ6563+[N II] $\lambda\lambda$6548, 6583 images in the direction perpendicular to the cones. The Hα λ6563+[N II] $\lambda\lambda$6548, 6583 emission arises almost entirely from an unresolved nuclear point source. Only very weak Hα λ6563+[N II] $\lambda\lambda$6548, 6583 emission is associated with the extended conical structure seen in [O III] λ5007. Terlevich et al. (1991) detect a nonstellar nuclear bar with a scale length $\sim$1″ in continuum light. They suggest that the bar may represent a truly extended BLR, and propose that the activity in the nucleus of NGC 4151 may result from a giant burst of star formation. They estimate that the half light radius, $R_{\rm eff}$, of the cluster undergoing the burst of star formation should be of order 9–30 pc ($R_{\rm eff} \approx 3$–$10R_c$, where R_c is the core radius of the cluster), or about 0.″18–0.″6 h^{-1} on the sky. The observed morphology of the nuclear emission is not compatible with this model, unless $R_{\rm eff} \sim R_c$ or R_c is considerably overestimated by Terlevich et al. (1991), since the dominant source of the Hα λ6563+[N II] $\lambda\lambda$6548, 6583 emission is the unresolved nuclear point source. Our data do not exclude the single supernova remnant starburst model of Terlevich et al.

© American Astronomical Society • Provided by the NASA Astrophysics Data System

1993ApJ...417...82E

PLATE 6

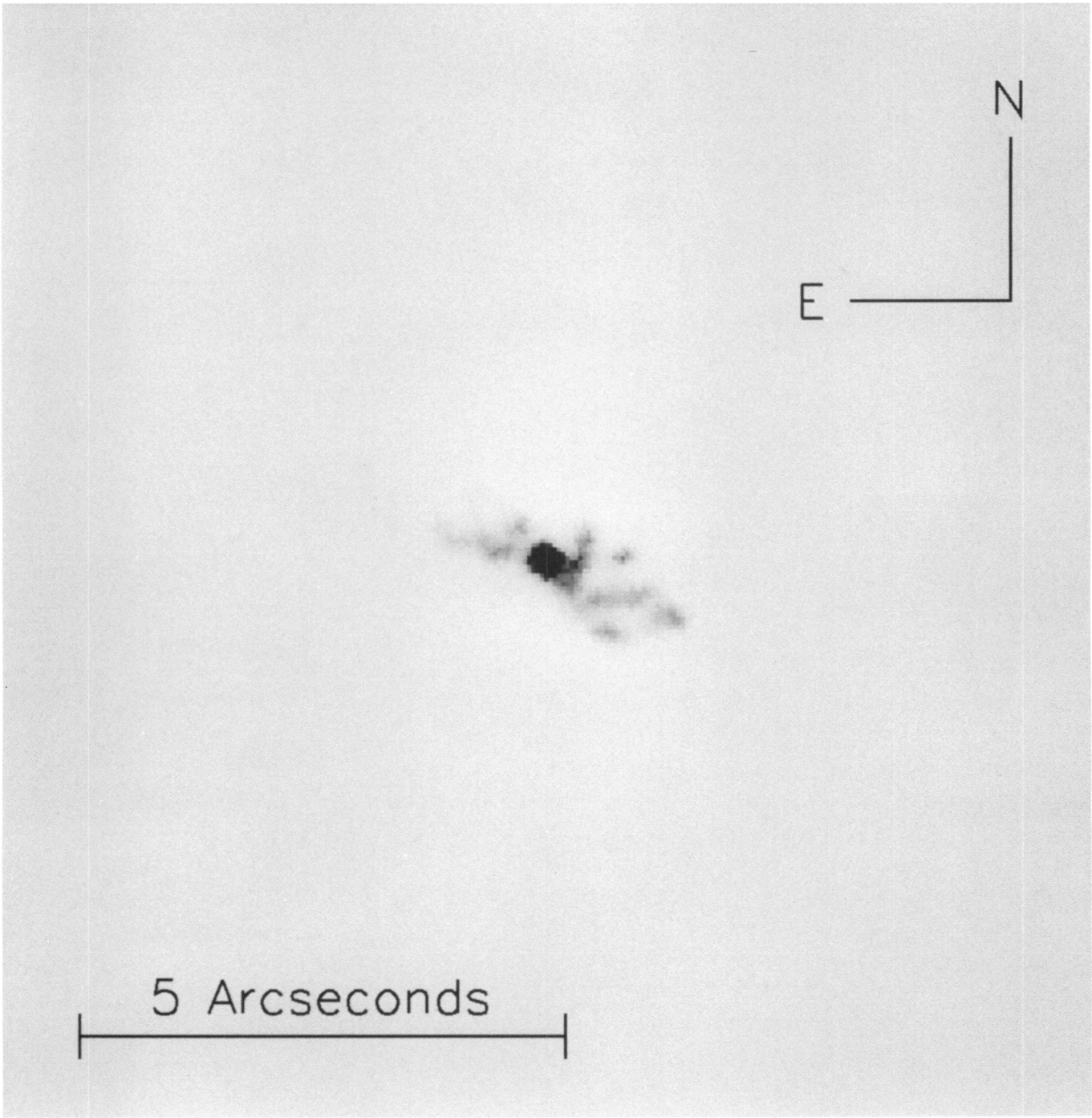

FIG. 7*a*

FIG. 7.—(*a*) Richardson-Lucy reconstruction of the continuum-subtracted [O III] λ5007 image sampled at the same pixel spacing as the original data, linearly scaled between 5% and 100% of the peak intensity of the extended emission. (*b*) same as (*a*), except that the image is linearly scaled between 5% and 40% of the peak intensity of the extended emission.

© American Astronomical Society • Provided by the NASA Astrophysics Data System

1993ApJ...417...82E

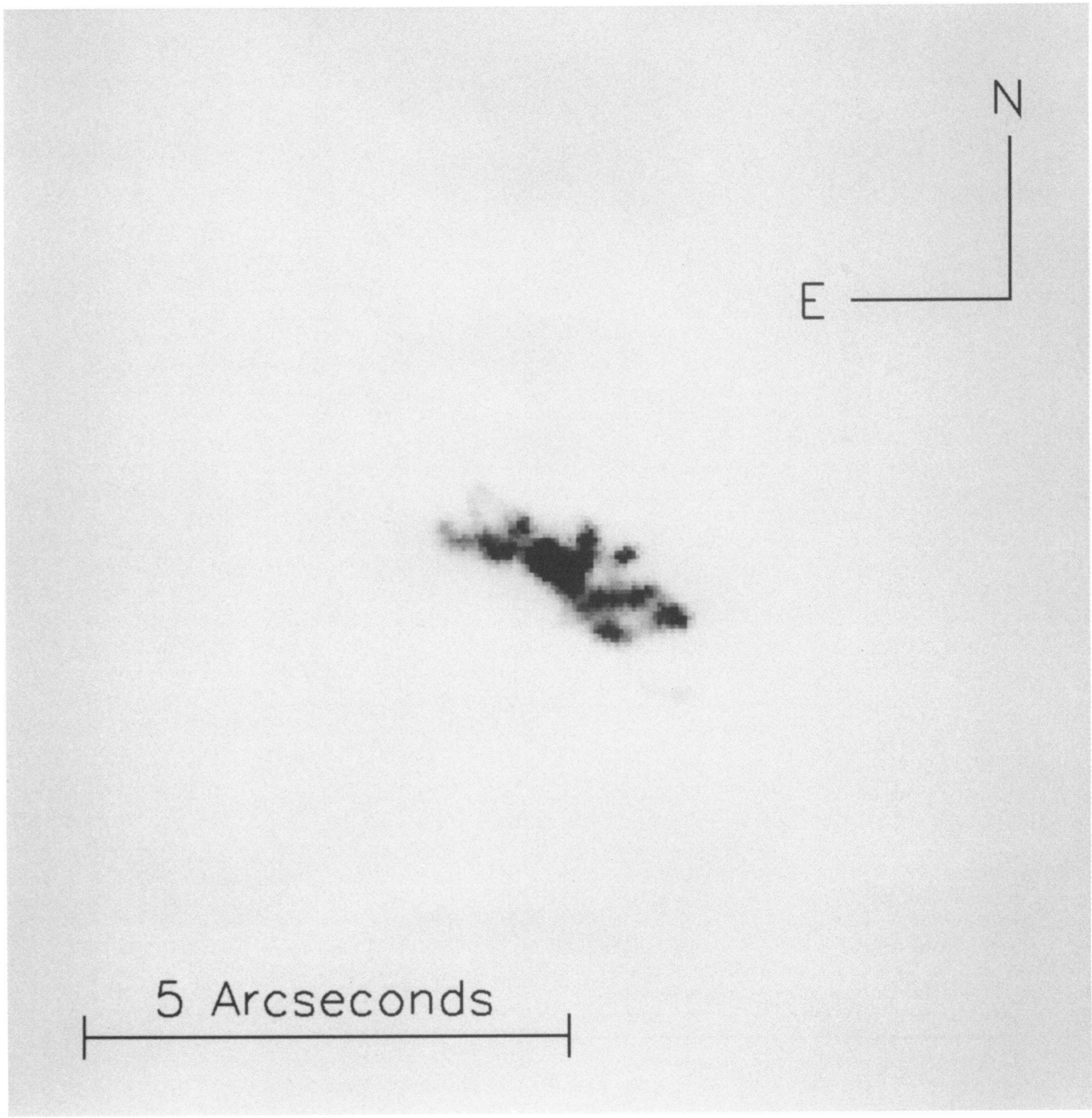

FIG. 7*b*

EVANS et al. (see 417, 84)

© American Astronomical Society • Provided by the NASA Astrophysics Data System

1993ApJ...417...82E

PLATE 8

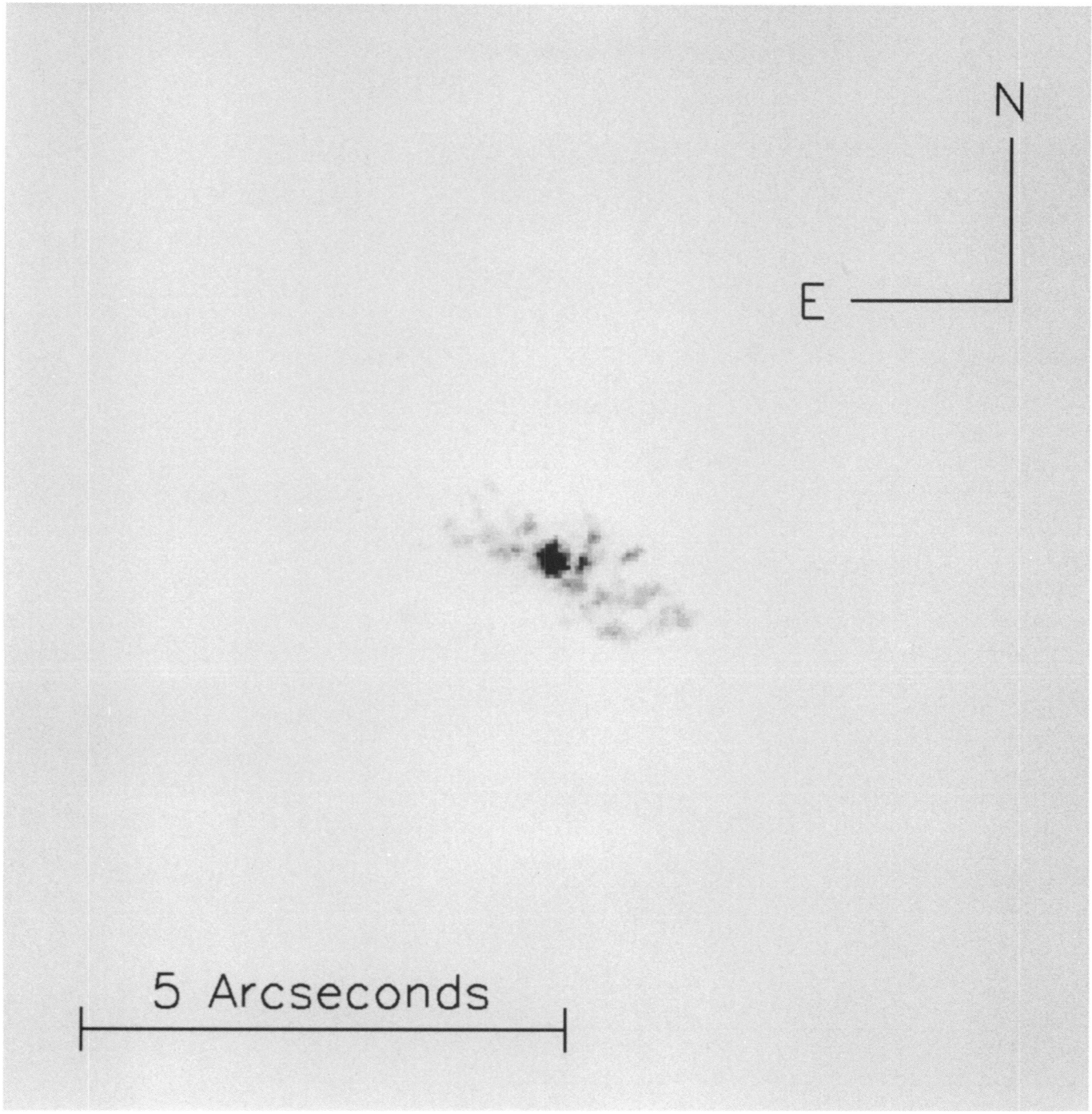

FIG. 8*a*

FIG. 8.—Same as Fig. 7, except that the MEM reconstruction is shown

© American Astronomical Society • Provided by the NASA Astrophysics Data System

1993ApJ...417...82E

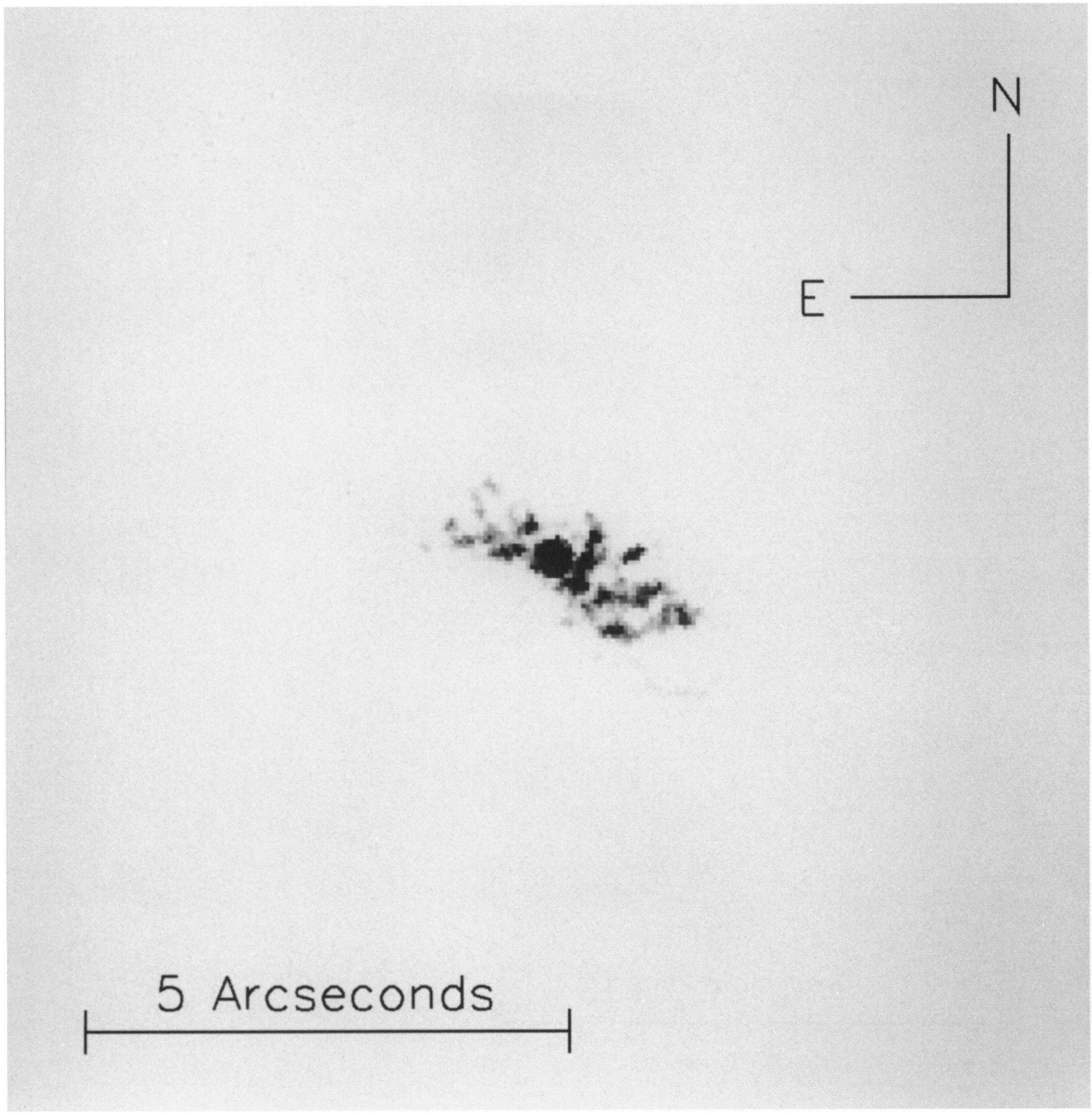

FIG. 8*b*

EVANS et al. (see 417, 84)

© American Astronomical Society • Provided by the NASA Astrophysics Data System

1993ApJ...417...82E

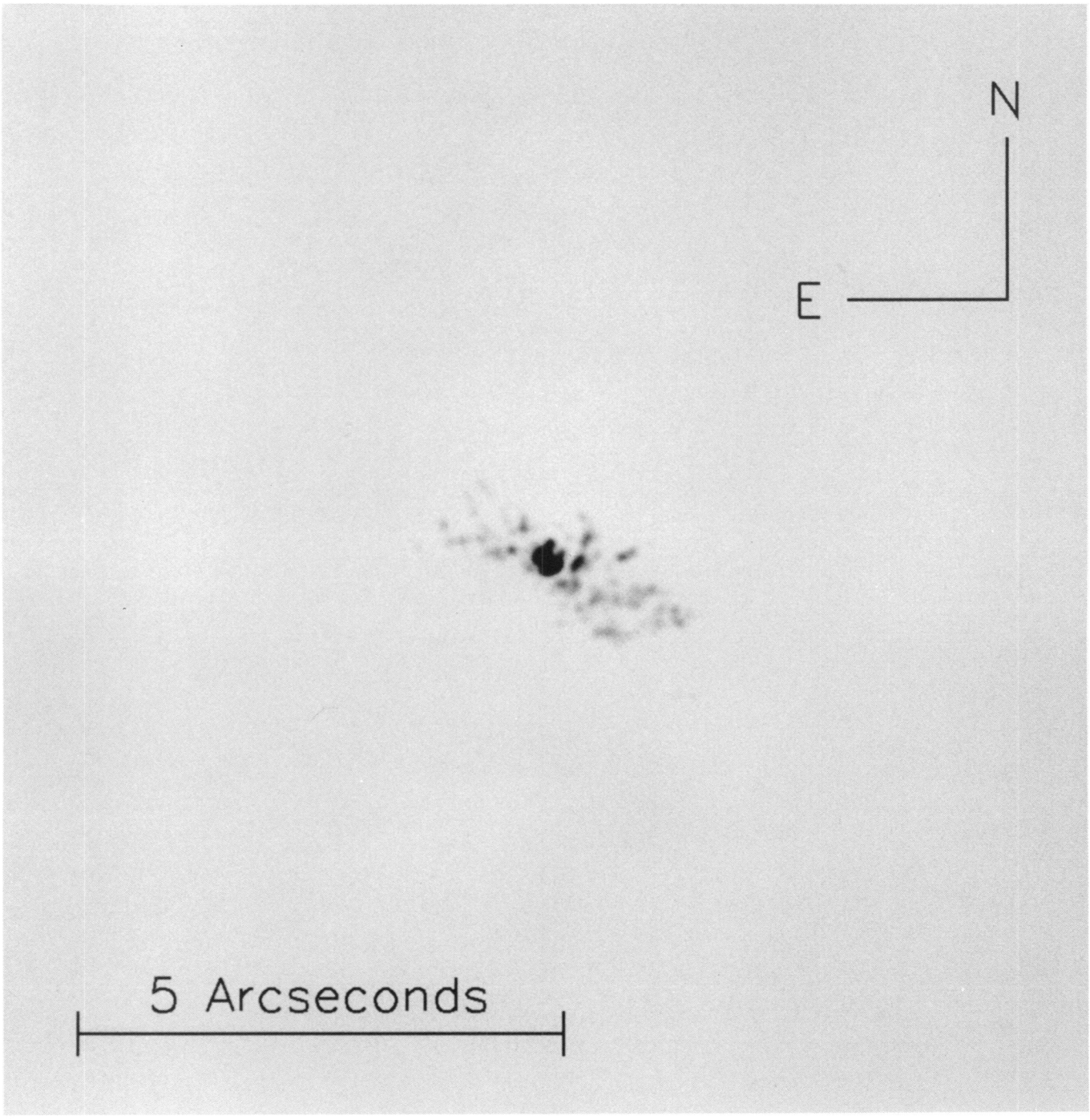

FIG. 9a

FIG. 9.—Same as Fig. 8, except that the reconstruction is sampled at 4 times the pixel sampling of that figure

© American Astronomical Society • Provided by the NASA Astrophysics Data System

1993ApJ...417...82E

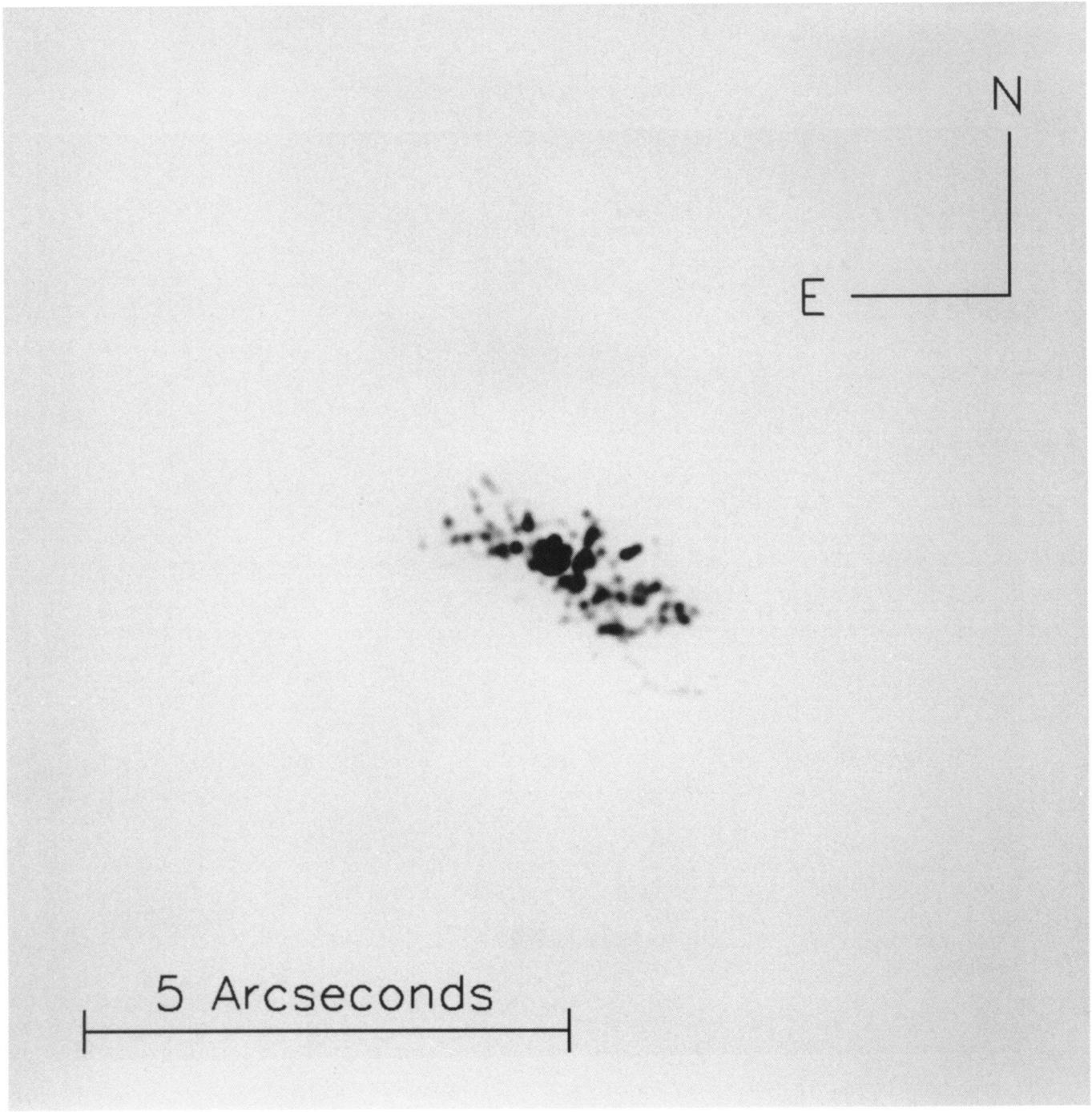

FIG. 9*b*

EVANS et al. (see 417, 84)

© American Astronomical Society • Provided by the NASA Astrophysics Data System

1993ApJ...417...82E

(1992), however, since in that model the size of the BLR is predicted to be ~ 0.01 pc.

The P.A. of the bar measured by Terlevich et al. (1991) is 150°, which is perpendicular to the P.A. of the axis of the nuclear emission-line cones. Based on the projected opening angle of the [O III] λ5007 emission, we conclude that it is not possible to explain the morphology of the nuclear NLR simply as a result of obscuration of a uniformly illuminated isotropic NLR by an optically thick bar that is exterior to the NLR and that has the observed properties. We will show below that the geometry of the ionization cones is not compatible with models invoking collimation of the nuclear ionizing radiation by a very optically thick torus. However, a model that incorporates a physically thin torus surrounded by a lower density atmosphere is consistent with our data. The feature seen by Terlevich et al. (1991) may be the shadow arising from such a torus. Another possibility is that the continuum image of the bar (seen by Terlevich et al. 1991) is contaminated by weak emission from low-ionization lines below our sensitivity limit. Low-ionization regions are expected perpendicular to the direction of collimation in several models that do not invoke a very optically thick torus, since the intensity of the nuclear ionizing field in these models is not automatically zero perpendicular to the direction of collimation.

Comparison of the [O III] λ5007 image of NGC 4151 with existing radio data does not show the degree of correspondence between the optical and radio emission seen in the nucleus of NGC 1068 (Evans et al. 1991) or in Markarian 3 (Tsvetanov et al. 1992). On arcsecond scales, the radio structure is extended in the general direction of the optical emission, but is distributed along P.A. 72°–84° (Johnston et al. 1982). This implies that it is misaligned by 12°–24° from our measured emission-line cone axis (P.A. 60°). The sub-arcsecond radio structure is similarly misaligned, since it has a position angle of 83° (Wilson & Ulvestad 1982). If we identify the unresolved core of the eastern radio lobe (which also has the flattest spectrum) with the nuclear point source, as suggested by Wilson & Ulvestad (1982), then the western lobe that is also visible in the VLBI data of Harrison et al. (1986) coincides with an [O III] λ5007 emission-line cloud. Although this suggests that there may be some relationship between the radio jet and the optical emission, the clear lack of strong radio emission explicitly associated with the rest of the observed NLR structure implies that the mechanical energy input by the radio jet does not dominate the energy balance of the interstellar medium in the nuclear region. A more interesting result is that the position angles of the elongation of the 1.6 and 5 GHz VLBI source ($\sim 57°$; Harrison et al. 1986; Preuss, Alef, & Pedlar 1987) and the 5 GHz MERLIN compact core ($\sim 62°$; Pedlar et al. 1992) *are* coincident with the measured axis of symmetry of the [O III] λ5007 emission-line cones. This suggests very strongly that a common mechanism may be responsible for the orientation of both the radio plasma ejected from the nucleus and the ionizing radiation field.

3.2. *Orientation and Geometry*

Heckman & Balick (1983) detected a narrow "string" of highly ionized emission-line knots forming part of the ENLR of NGC 4151. This string is visible in [O III] λ5007 and Hα λ6563 emission, and extends $\sim 18''$ SW of the nucleus. Schulz (1988) traced the string further out to a distance of $\sim 30''$ from the nucleus, and has shown that the local gas velocities of the ionized hydrogen in the string coincide with the gas velocities of the H I disk. This velocity coincidence implies that the string must lie in the disk of the galaxy. Pérez-Fournon & Wilson (1990) further demonstrate, based on the measurements of the disk major axis (P.A. = 26°; Davies 1973; Simkin 1975) and inclination ($i = 21°$; Simkin 1975), that the string is almost in the plane of the sky, and tilted slightly away from us (the inclination of the string to our line of sight is $\sim 98°$).

Although the string P.A. (228°) is close to the P.A. of the nuclear cones, there is no reason to assume that the inclination of the cone axis to our line of sight is similar to that inferred for the string. In order that the string be ionized by the same radiation field responsible for the nuclear emission-line cones, all that is required is that the string fall *somewhere* within the volume of the ionization cone. Schulz (1990) observes that the [O III] λ5007 line is split into a double profile within $\sim 4''$ of the nucleus, with one component at the local disk velocity, and a second component which is redshifted to the NE of the nucleus and blueshifted to the SW. If outflow is dominant in this region, as Schulz (1990) suggests, this implies that the SW cone is directed toward us and the NE cone is directed away from us. This geometry is also suggested by the fact that the observed emission-line filaments in the SW cone are typically brighter and extend out to a somewhat larger radius from the nucleus than their counterparts in the NE cone. The latter suggests that perhaps the NE cone may be somewhat obscured along our line of sight, possibly as a result of the intervening galactic disk in NGC 4151.

One possible explanation for the difference between the large opening angle we measure and the value inferred at larger radii is that the gas density in the cone is significantly lower at distances of a few tens of pc from the nucleus along most radial directions. This can naturally occur if the ionized gas is confined to the disk of NGC 4151. If the cone axis is inclined substantially to our line of sight, as we discuss below, then the gas which may be ionized by the central source will be restricted by the scale height of the matter in the disk of NGC 4151. Near the nucleus the cones of ionizing radiation will be filled with gas, and a wide opening angle will be measured as shown in our high-resolution images. At larger distances the cones may not be filled, producing the smaller opening angles measured in ground-based images.

From our measured cone opening angle projected onto the plane of the sky, together with the assumption described above that the string lies both in the plane of the galaxy and also within the SW ionizing cone, the minimum inclination angle of the cone axis to our line of sight can be determined from the equation

$$\sin^2(\theta/2) = \sin^2(\chi) + \tan^2(\xi - \varphi)\cos^2(\theta/2),$$

where $\tan(\theta/2) = \tan(\theta'/2)\sin\varphi$, and $\tan(\chi) = \tan(\chi')\sin\xi$. In these equations, θ' and θ are the cone opening angle projected onto the plane of the sky and the actual cone opening angle, respectively, χ' and χ are the projected and actual angular separation of the position angles of the cone axis and the string, respectively, ξ is the angle of inclination to our line of sight of the string, and φ is the angle of inclination to our line of sight of the cone axis.

The geometry that minimizes the deviation between our line of sight and the nearest edge of the cone places the string along the far edge of the SW ionization cone. With these assumptions, $\theta' \sim 75°$, $\chi' \sim 12°$, $\xi \sim 98°$, and we derive a value for the inclination of the cone axis to our line of sight of $\varphi \sim 65°$ and

© American Astronomical Society • Provided by the NASA Astrophysics Data System

1993ApJ...417...82E

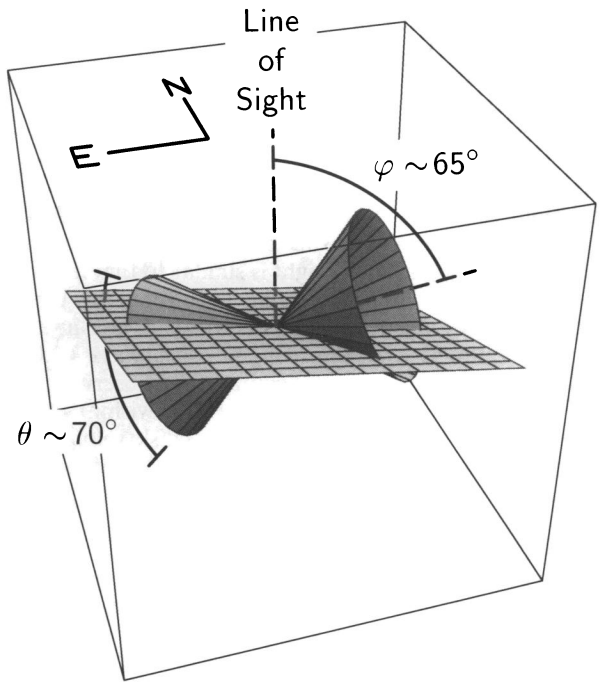

FIG. 10*a*

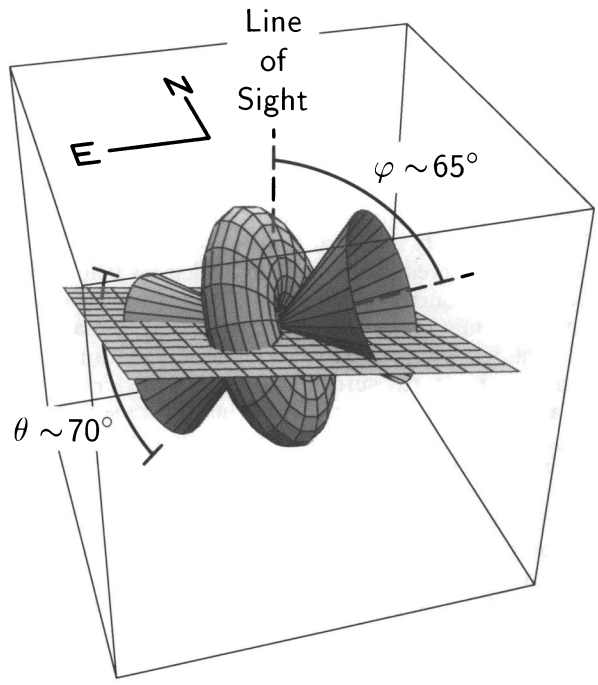

FIG. 10*b*

FIG. 10.—(*a*) Geometry of the emission-line cones in NGC 4151 that is most compatible with the observational data. (*b*) Same as (*a*), with a simple geometric torus superposed, demonstrating that the line of sight must intersect the torus.

an actual cone opening angle of $\theta \sim 70°$. A model of this geometry to aid visualization is presented in Figure 10*a*. The inclination φ of the cone axis can be larger than this if the string falls totally within the cone instead of along the far edge, but it cannot be smaller if the string is contained within the ionization cone. This geometry implies that the minimum angle between our line of sight and the edge of the ionizing cone closest to our line of sight is $\sim 30°$.

The large inclination angle we derive for the cone axis is in excellent agreement with previous studies of the broad-line region and of the X-ray source in NGC 4151. Maoz et al. (1991) conclude from optical monitoring observations of the continuum and broad Balmer lines in NGC 4151 that the broad Balmer-line light curve is best reproduced by an edge-on disk BLR model. Ulrich et al. (1985) have argued that the UV L1 λ1518 and L2 λ1594 emission-line features are Doppler-shifted C IV λ1550 lines that are excited by a two-sided SS 443-like jet impinging on clouds in the region where the ultra-broad C IV λ1550 line is formed. If this interpretation is correct, then the observed correlation of the short time variability of the L1 and L2 lines would constrain the jet to lie almost in the plane of the sky. Although the best fit to the narrow profile of the Fe Kα observed by BBXRT (Weaver et al. 1992) is for a model accretion disk that is face-on, the lack of a correlation between the flux variability of the Fe Kα line and the continuum argues that this line arises in the BLR, rather than from the accretion disk. Therefore this observation places no constraints on the geometry of the accretion disk. A search for Compton reflection features from the accretion disk in the X-ray spectrum of NGC 4151 (Maisack & Yaqoob 1991) finds that the maximum contribution of a reflected component is smaller than 47% of the value that would be expected under the assumption that half of the primary radiation has been reprocessed. Maisack & Yaqoob (1991) interpret the lack of evidence for a strong reflected component as being caused by a nearly edge-on geometry for the accretion disk as seen along our line of sight.

3.3. *Implications for Unified Models*

The inferred orientation for the ionization cones has strong implications for models attempting to explain the nuclear emission-line morphology in NGC 4151 within the framework of the unified model of AGN. For Seyfert galaxies, the most popular collimating scenario invokes a small, very optically thick molecular torus surrounding the nuclear engine. The torus both collimates the ionizing radiation and either reveals (Seyfert 1) or obscures (Seyfert 2) the central ionizing source and the BLR, depending on the orientation to the line of sight to the observer. Lines of sight exterior to the cones defined by the shadow of the torus will see cones of emission line gas projected onto the sky, while views interior to the cone will see gas illuminated at all position angles around the central source. Thus cones of emission line gas should be found in Seyfert 2 galaxies (e.g., Pogge 1989; Evans et al. 1991) while Seyfert 1's should exhibit more isotropic distributions of ionized gas (Pogge 1989; Kinney et al. 1992; Boksenberg 1993). In the case of NGC 4151, however, we have a relatively unobstructed view of the BLR and the continuum source, suggesting that we have a direct view of the nuclear regions interior to the cone of this Seyfert 1, yet we see a well defined biconical structure for the emission line gas which argues that our line of sight must lie in the shadowed region as in Seyfert 2 galaxies.

Although our line of sight to the nuclear regions of NGC 4151 is relatively clear, it is not totally unobstructed. The central 0.5–5 keV X-ray source is partially covered by absorbing material with a line-of-sight column density $N_H \sim 5$–15

© American Astronomical Society • Provided by the NASA Astrophysics Data System

1993ApJ...417...82E

$\times 10^{22}$ cm^{-2} over $\sim$90% of the source (e.g., Barr et al. 1977; Mushotzky, Holt, & Serlemitsos 1978; Holt et al. 1980). The ultraviolet continuum appears to have relatively low extinction ($E_{B-V} < 0.10$; Penston et al. 1981; Kriss et al. 1992), but numerous absorption lines cover *both* the continuum and the broad emission lines at optical and ultraviolet wavelengths (Anderson 1974; Penston et al. 1981; Bromage et al. 1985; Kriss et al. 1992). The UV absorbing gas has a much lower total column density than the X-ray absorbing material, and it is dominated by outflowing dense ($n_e > 10^{9.5}$ cm^{-3}) gas with a high effective Doppler parameter ($b \sim 200$ km s^{-1}), a total equivalent hydrogen column density of $N_{\rm H} \sim 10^{21}$ cm^{-2} (Bromage et al. 1985; Kriss et al. 1992), and a neutral hydrogen component with $N_{\rm H} \sim 10^{18}$–10^{21} cm^{-2} (Kriss et al. 1992). A successful model for NGC 4151 must not only explain how the radiation is collimated to produce the observed biconical emission line structure, but must also explain our only partially obscured view of the BLR and continuum source, and the differing column densities for UV and X-ray absorption along our line of sight.

The simplest unified models in which an infinitely optically thick torus collimates the radiation field can be ruled out using geometrical arguments. To detect simultaneously the point source BLR and observe collimated ionization cones, it is necessary that the source responsible for the bulk of the ionizing radiation be smaller than the size of the BLR so that it is possible to see the latter directly over the edge of the torus while the former remains largely obscured. Since the size of the BLR in NGC 4151 is a few light days across (Peterson & Cota 1988; Clavel et al. 1990), and the size of the source of the ionizing continuum inferred from the X-ray variability time scale is roughly an order of magnitude smaller (Mushotzky et al. 1978; Lawrence 1980), at first glance such a geometry appears feasible. For an infinitely optically thick torus (see Fig. 10*b*), the maximum angle between our line of sight and the edge of the ionization cone, $\zeta_{\rm max}$, that will enable us to observe the BLR directly is determined purely by geometrical shadowing. If $r_{\rm cont}$ is the radius of the source responsible for the ionizing continuum, $r_{\rm BLR}$ is the BLR radius, and r_t is the inner radius of the torus, then

$$\frac{r_{\rm BLR}}{\sin(\theta/2 + \zeta_{\rm max})} - \frac{r_{\rm cont}}{\sin(\theta/2)} = r_t[\cot(\theta/2) - \cot(\theta/2 + \zeta_{\rm max})] .$$

The inner radius of the molecular torus is expected to be of the order of a few times the characteristic scale length, S, of the accretion region (Krolik & Begelman 1988, eq. [35]), and is controlled by the equilibrium balance between the mass-loss rate by ablation from the inner edge of the torus and the mass inflow from further out in the galaxy. With the same assumptions as Krolik & Begelman (1988), we estimate that $S \sim 0.05$ pc for NGC 4151, and therefore that $r_t \sim 0.2$ pc, were we have taken the mean ionizing luminosity[4] to be $\sim 2.1 \times 10^{43}$ ergs s^{-1}. Substituting the values estimated above for the unknowns in the last equation yields a maximum possible value $\zeta_{\rm max} \lesssim 1°$, substantially smaller than the angle estimated directly from the observations ($\zeta_{\rm obs} \sim 30°$).

More complex geometries than that shown in Figure 10 are possible, but for any given θ and r_t, varying the torus geometry will alter $\zeta_{\rm max}$ by a factor only of order unity. For the very optically thick molecular torus model, where the column density through the equatorial plane of the torus is $\gtrsim 10^{24}$ cm^{-2}, we would expect for lines of sight corresponding to $\zeta_{\rm obs} \gg \zeta_{\rm max}$ (as is the case for NGC 4151) that the optical depth to the BLR for visible and near UV photons should be substantially greater than unity, and therefore the BLR should not be visible directly. In addition, such lines of sight would have an effective hydrogen column density considerably higher than the observational value derived from either the UV absorption lines or the X-ray data. It may be possible to ameliorate these constraints somewhat by considering a geometry in which the string is tilted toward us in a physically thick galaxian disk. However, as the inclination of the cone axis decreases, the actual cone opening angle for a given measured opening angle projected on the plane of the sky also decreases. Our observations suggest, therefore, that an acceptable geometry for a very optically thick molecular torus model is highly improbable unless we assume that the disk scale height is unreasonably large ($\sim$1 kpc).

While a very optically thick torus cannot collimate the radiation field in NGC 4151, we cannot rule out the presence of a molecular torus as originally argued by Penston et al. (1990). They suggest that if the central source emits ionizing photons isotropically, then reradiation of photons absorbed by the molecular torus would result in a far-infrared luminosity considerably higher than observed. The larger cone opening angle we measure does not affect their argument substantially because the area of the sky subtended by the absorbing material only decreases by $\sim$15% (the unabsorbed area subtended by the ionizing cones estimated from our data is $\sim$18% vs. $\sim$1%–2% assumed by Penston et al. 1990). However, Pier & Krolik (1991, 1992) have recently shown that reradiation of infrared flux in the molecular torus model occurs substantially anisotropically as a function of viewing angle, with the maximum flux visible when the torus is face on. This is consistent with the results of Storchi-Bergmann, Mulchaey, & Wilson (1992), who find that the observed *IRAS* luminosities are consistent with the torus model in eight of the nine Seyfert 2 galaxies with well defined radiation cones they studied. Given our best estimate of the inclination of the axis of the torus, above, we conclude that the Penston et al. (1990) estimate of the total infrared luminosity cannot be used to exclude a molecular torus model for NGC 4151.

A simple modification of the very optically thick molecular torus model that provides effective collimation of ionizing radiation while leaving a relatively clear line of sight to the nucleus and BLR is a geometry with a physically thin, dense molecular torus, surrounded by a lower column density "atmosphere" of neutral or nearly neutral gas through which our line of sight passes. The conditions near the inner edge of the molecular torus may be quite conducive to the formation of just such an atmosphere. Heating resulting from the X-rays responsible for ablating the inner surface of the torus may inflate or "puff-up" the inner region of the molecular gas, thus creating the lower column density atmosphere required. In this model, the edges of the *ionization* cones will be determined by the angle at which the path through the atmosphere gives a column density sufficient to block the ionizing ultraviolet. Columns with $N_{\rm H} = 10^{20}$ cm^{-2} will be optically thick at all wavelengths past the Lyman edge up to the soft X-ray. Above the Lyman limit, and for normal dust-to-gas ratios, extinction will not have much impact until gas column densities exceed several times 10^{21}

[4] This luminosity is the integral from 13.6 eV to 25 keV of the extinction-corrected ultraviolet power-law spectrum of Kriss et al. (1992) extrapolated to the soft X-ray where it meets the mean absorption-corrected X-ray spectrum of Perola et al. (1982).

© American Astronomical Society • Provided by the NASA Astrophysics Data System

1993ApJ...417...82E

cm^{-2}. Consequently, lines of sight falling within the cones defined by the *shadow* of the opaque torus, but exterior to the *ionization* cones, will have a relatively clear view of the central regions at wavelengths longward of the Lyman edge. This thin atmosphere around the torus can explain the UV absorption lines and the low extinction to the UV continuum, but it is insufficient to account for the X-ray absorption.

Higher column density material inside the inner edge of the torus, for example the BLR clouds, can explain the X-ray absorption provided it is highly ionized, so that it is transparent to the ionizing ultraviolet, and hot, so that dust does not obscure the optical and UV continuum. If the high column density material is not fully ionized, for example if the BLR clouds are sufficiently optically thick that the backside of the clouds has a substantial neutral fraction, then the clouds may be opaque to the ionizing ultraviolet continuum. In this case, the thin atmosphere would still produce the observed UV absorption lines and provide a low extinction line of sight to the UV continuum. However, the location of the edges of the ionization cones would no longer be determined by the optical depth to the ionizing UV through the torus's atmosphere, but rather would be fixed by the optical depth of the material interior to the torus.

A variation of the torus-plus-atmosphere geometry is a clumpy torus comprised of clouds of both high- and low-density gas. If the filling factor for the dense regions is low enough, then many lines of sight will have low column density holes with a clear view of the BLR and the continuum source. Dynamical motions in the torus that produce changes in the optical depth would give variability time scales of months to years. This is insufficient, however, to account for the rapid variability that occurs on time scales of hours for the X-ray continuum (Mushotzky, Holt, & Serlemitsos 1978; Lawrence 1980), and days to weeks for the optical continuum and broad lines (Antonucci & Cohen 1983; Ulrich et al. 1984; Clavel et al. 1991). Unless we are in a very fortuitous situation as a preferred observer, however, one would expect many such holes in the torus. This is not inconsistent with our observation of a well defined biconical structure provided each hole has sufficient column density to be optically thick to ionizing UV radiation.

Another mechanism for collimating the radiation that completely dispenses with any role for the obscuring torus is a flattened configuration of broad-line clouds. Ferland & Mushotzky (1982) proposed broad-line clouds as the source of the X-ray absorption and the soft X-ray variability of NGC 4151, and this idea was further developed by Reichert et al. (1985) and Yaqoob & Warwick (1991). In this description the central nuclear source is obscured by many broad-line clouds which cover $\sim 90\%$ of the continuum source. The thermal line widths of these BLR clouds, the small fraction of the continuum covered by an individual cloud, and the broad velocity distribution of the BLR, would give rise to only weak, shallow absorption features in the UV. The observed UV absorption lines require full coverage of both the BLR and the continuum source by highly turbulent, outflowing material (Bromage et al. 1985; Kriss et al. 1992). This can be explained by radiatively accelerated, turbulent clumps of disintegrating broad-line clouds on the outer edge of the BLR (Kriss et al. 1992). If the BLR has a flattened configuration as suggested by the Balmer line reverberation mapping of Maoz et al. (1991), it can effectively collimate the ionizing radiation. In this case, the opacity in the plane of the clouds would be high enough to block ionizing photons in that direction, but still allow them to escape in a direction which is perpendicular to the plane of the disk. Pérez-Fournon & Wilson (1990) argue that the disklike distribution of broad-line clouds could be detected by searching for double-peaked line profiles. However, a disklike geometry does not require disklike kinematics. If the BLR is collimating the radiation, it must be fairly thick to cast a shadow with an opening angle of 70°. This would imply a substantial vertical component to the velocity ellipsoid. In addition, if the UV absorption lines are associated with gas outflowing from the BLR as suggested by Kriss et al. (1992), there will be a substantial radial component as well. Therefore the lack of observed double-peaked line profiles does not necessarily exclude this explanation.

A final mechanism we consider for collimating the ionizing radiation is that the continuum radiation pattern is inherently anisotropic. This has been advocated by Miller, Goodrich, & Matthews (1991) as a distinct possibility in NGC 1068. All the absorption mechanisms we have discussed above would still be applicable in NGC 4151, but the torus and the BLR are decoupled from playing any role in collimating the radiation, and they need not even be axisymmetric with the radiation pattern, as suggested by Miller, Goodrich, & Matthews.

A possible source of inherently anisotropic radiation could be a "naked" thick accretion disk around a supermassive black hole (Penston et al. 1990; Pérez-Fournon & Wilson 1990). The theoretical models presented by Madau (1988) predict a somewhat narrower cone opening angle than we observe in NGC 4151. However, the parameters used in the numerical calculations by Madau (1988) are more appropriate to higher luminosity quasars than to NGC 4151. The cone opening angle predicted by the model can be readily increased to the observed value by decreasing the black hole mass and possibly also increasing the size of the accretion disk. A black hole mass of order $\sim 10^6\ M_\odot$ is required to match the model to the luminosity of NGC 4151, while a change of order unity is all that is required for the accretion disk radius (Madau 1992).

The radiation pattern from a thick accretion disk does not have sharp edges, however, and lines of sight outside of the ionization cones are still exposed to ionizing radiation although at greatly reduced intensity. Faint emission may be produced from clouds outside of the bright cones, and inspection of Figures 7–9 suggests that there may be some evidence for this. The spectrum of the ionizing radiation changes rapidly away from the center of the cones, and spatially resolved spectra of individual clouds that would permit one to infer the shape of the incident spectrum may help to test this possibility.

4. SUMMARY AND CONCLUSIONS

We have used the PC aboard *HST* to obtain high spatial resolution [O III] $\lambda 5007$ and Hα $\lambda 6563$ + [N II] $\lambda\lambda 6548$, 6583 images of the nucleus of NGC 4151. The observed Hα $\lambda 6563$ + [N II] $\lambda\lambda 6548$, 6583 emission arises from an unresolved nuclear point source, presumably associated with the BLR. The [O III] $\lambda 5007$ image resolves the NLR into a number of emission-like clouds with a stringy morphology. These are distributed in a biconical structure with apices coincident with the central point source and a cone opening angle projected on the sky of $\sim 75° \pm 10°$. The cone position angle of 60°/240° $\pm$ 5° is aligned with the extension of the nuclear VLBI radio source, suggesting that the same mechanism may align both the optical ionizing radiation field and the pc scale radio

© American Astronomical Society • Provided by the NASA Astrophysics Data System

1993ApJ...417...82E

structure. Although the western radio lobe does appear to be associated with a region of [O III] λ5007 emission, most of the emission-line clouds do not have associated radio emission.

We infer a geometry from these data that is incompatible with the simplest version of the unified model of AGNs that invokes a very optically thick molecular torus surrounding the BLR to obscure the source of ionizing photons, and which depends solely on the inclination of the torus to our line of sight to differentiate between objects with and without broad-line emission. In particular, the standard unified model that has been suggested to apply to NGC 1068 does not appear to be a viable explanation for NGC 4151. Our data indicate that for feasible model parameters our line of sight must lie outside of the ionization cones, and therefore the very optically thick molecular torus model would predict that the central broad-line point source should not be visible directly. Our data are compatible with models of obscuration that have an effective neutral hydrogen column density along our line of sight of no more than $\lesssim 10^{21}$ cm^{-2}.

Possible mechanisms for collimating the radiation in NGC 4151 include (1) a very optically thick torus surrounded by a lower density atmosphere that collimates the ionizing radiation but leaves the line of sight to the nucleus relatively unobscured; (2) BLR clouds that are located in a disk geometry so that their opacity absorbs much of the ionizing radiation emitted in the disk plane; and (3) anisotropic ionizing radiation from a thick accretion disk surrounding a black hole as a mechanism for forming the cones. We cannot distinguish among these possibilities using these data alone.

The authors would like to acknowledge useful discussions with Julian Krolik, Andrew Lawrence, Piero Madau, Richard Mushotzky, Hartmut Schulz, Susan Simkin, Martin Ward, Kim Weaver, and Andrew Wilson. We would also like to thank Lee Armus, who performed the alignment of the emission-line and continuum frames, and the continuum subtraction. This work was supported in part by NASA grant NAG5-1630.

REFERENCES

Anderson, K. S. 1974, ApJ, 189, 195
Antonucci, R. R. J., & Cohen, R. D. 1983, ApJ, 271, 564
Antonucci, R. R. J., & Miller, J. S. 1985, ApJ, 297, 621
Barr, P., White, N. E., Sanford, P. W., & Ives, J. C. 1977, MNRAS, 181, 43P
Barthel, P. D. 1989, ApJ, 336, 606
Boksenberg, A. 1993, in The Nature of Compact Objects in AGN, ed. A. Robinson & R. J. Terlevich, (Cambridge: Cambridge Univ. Press), in press
Bromage, G. E., et al.1985, MNRAS, 215, 1
Clavel, J., et al. 1990, MNRAS, 246, 668
———. 1991, ApJ, 366, 64
Davies, R. D. 1973, MNRAS, 161, 25P
Evans, I. N.,Ford, H. C., Kinney, A. L., Antonucci, R. R. J., Armus, L., & Caganoff, S. 1991, ApJ, 369, L27
Ferland, G. J., & Mushotzky, R. F. 1982, ApJ, 262, 564
Gull, S. F., & Skilling, J. 1991, Quantified Maximum Entropy "MEMSYS 5" Users' Manual, Version 1.10 (Royston: Maximum Entropy Data Consultants Ltd.)
Harrison, B., Pedlar, A., Unger, S. W., Burgess, P., Graham, D. A., & Preuss, E. 1986, MNRAS, 218, 775
Heckman, T. M., & Balick, B. 1983, ApJ, 268, 102
Holt, S. S., et al. 1980, ApJ, 241, L13
Johnston, K. J., Elvis, M., Kjer, D., & Shen, B. S. P. 1982, ApJ, 262, 61
Kinney, A., et al. 1992, BAAS, 24, 727
Kriss, G. A., et al.1992, ApJ, 393, 485
———. 1993, in Proc. 8th IAP Meeting, First Light in the Universe: Stars or QSOs, ed. B. Rocca-Volmerange, et al. (Paris: Editions Frontières), in press
Krist, J. 1992, The Tiny Tim User's Manual, version 1.01 (Baltimore: STScI)
Krolik, J. H., & Begelman, M. C. 1986, ApJ, 308, L55
———. 1988, ApJ, 329, 702
Krolik, J. H., & Lepp, S. 1989, ApJ, 347, 179
Lauer, T. R. 1989, PASP, 101, 445
Lawrence, A. 1980, MNRAS, 192, 83
———. 1987, PASP, 99, 309
Lawrence, A., & Elvis, M. 1982, ApJ, 256, 410
Lucy L. 1974, AJ, 79, 745
Madau, P. 1988, ApJ, 327, 116
———. 1992, private communication
Maisack, M., & Yaqoob, T. 1991, A&A, 249, 25
Maoz, S., et al. 1991, ApJ, 367, 493
Miller, J. S., & Goodrich, R. W. 1990, ApJ, 355, 456
Miller, J. S., Goodrich, R. W., & Matthews, W. G. 1991, ApJ, 378, 47
Mushotzky, R. F., Holt, S. S., & Serlemitsos, P. J. 1978, ApJ, 225, L115
Osterbrock, D. E., & Koski, A. T. 1976, MNRAS, 176, 61P
Pedlar, A., et al. 1992, preprint
Penston, M. V., et al. 1981, MNRAS, 196, 857
———. 1990, A&A, 236, 53
Pérez, E., González-Delgado, R. M., Tadhunter, C., & Tsvetanov, Z. 1989, MNRAS, 241, 31P
Pérez-Fournon, I., & Wilson, A. S. 1990, ApJ, 356, 456
Perola, G. C., et al. 1982, MNRAS, 200, 293
Peterson, B. M., & Cota, S. A. 1988, ApJ, 330, 111
Pier, E. A., & Krolik, J. H. 1991, BAAS, 23, 1469
———. 1992, ApJ, 401, 99
Pogge, R. W. 1989, ApJ, 345, 730
Pogge, R. W., & de Robertis, M. M. 1993, ApJ, 404, 563
Preuss, E., Alef, W., & Pedlar, A. 1987, in IAU Symp. 121, Observational Evidence of Activity in Galaxies, ed. E. Ye. Khachikian (Dordrecht: Reidel), 269
Reichert, G. A., Mushotzky, R. F., Petre, R., & Holt, S. S. 1985, ApJ, 296, 69
Richardson, W. H. 1972, J. Opt. Soc. Am., 62, 55
Schulz, H. 1987, A&A, 178, 7
———. 1988, A&A, 203, 233
———. 1990, AJ,1442
Simkin, S. M. 1975, ApJ, 200, 567
Storchi-Bergmann, T., Mulchaey, J. S., & Wilson, A. S. 1992, ApJ, 395, L73
Tadhunter, C. N., & Tsvetanov, Z. 1989, Nature, 341, 422
Terlevich, R., Sánchez Portal, M., Díaz, A. I., & Terlevich, E. 1991, MNRAS, 249, 36
Terlevich, R., Tenorio-Tagle, G., Franco, J., & Melnick, J. 1992, MNRAS, 255, 713
Tsvetanov, Z., et al. 1992, BAAS, 24, 751
Ulrich, M.-H. 1973, ApJ, 181, 51
Ulrich, M.-H., et al. 1984, MNRAS, 206, 221
———. 1985, Nature, 313, 745
Weaver, K., et al. 1992, ApJ, 401, L11
Wilson, A. S., & Ulvestad, J. S. 1982, ApJ, 263, 576
Wilson, A. S., Ward, M. J., & Hanniff, C. A. 1988, ApJ, 334, 121
Yaqoob, T., & Warwick, R. S. 1991, MNRAS, 248, 773

© American Astronomical Society • Provided by the NASA Astrophysics Data System